Anal. Chem. **2004,** *76,* 2071−2082

Parallel, Quantitative Measurement of Protein Binding to a 120-Element Double-Stranded DNA Array in Real Time Using Surface Plasmon Resonance Microscopy

Jennifer S. Shumaker-Parry,[†,‡] Ruedi Aebersold,[§] and Charles T. Campbell*[,†]

Department of Chemistry, University of Washington, Seattle, Washington 98195-1700, and Institute for Systems Biology, 1441 North 34th Street, Seattle, Washington 98103-8904

Quantitative, real-time measurement of kinetics of sequence-specific binding of DNA-binding proteins to double-stranded DNA (dsDNA) immobilized in a 10 × 12 array on a planar gold surface is demonstrated using surface plasmon resonance (SPR) microscopy. This binding of the yeast transcription factor Gal4 to a 120-spot dsDNA array made with alternating 200-μm spots of its dsDNA operator sequence and an unrelated DNA sequence proves that this method could be used to *simultaneously* monitor the kinetics of binding of proteins to 120 different dsDNA sequences with a sensitivity to ~0.5 pg (<2 × 10^7 molecules) of bound protein in each array spot at a time resolution of 1 s. The method is label free and also allows absolute quantitative determination of the binding stoichiometry (i.e., the number of proteins bound per dsDNA) at each time. The dsDNA array was fabricated using a robotic microspotting system to deliver nanoliter droplets of biotinylated dsDNA solutions onto a streptavidin linker layer immobilized with biotinylated alkylthiols on a thin gold film. Simultaneous monitoring of binding to the many array elements allows the use of reference spots (i.e., array elements with unrelated dsDNA sequences) to correct the signal for nonspecific protein−DNA binding and changes in bulk refractive index of the solutions in the SPR microscope's flow cell. This allows high-throughput analyses of the kinetics and equilibrium of protein−dsDNA binding.

Protein−DNA interactions are of fundamental importance in biology and medicine. One of the largest and most diverse classes of DNA-binding proteins is the transcription factor.[1] Activity of transcription factors in a cell determines the transcription rate of each expressed gene and thus controls basic biological processes including cell replication, differentiation, and development.[1−4] These proteins bind to sequence-specific double-stranded DNA (dsDNA) sites with differing degrees of specificity and strength and may act alone or cooperatively with other proteins to regulate gene expression. Understanding the molecular mechanisms of gene expression in eukaryotes requires a precise knowledge of the strength and specificity of these protein−dsDNA interactions.[1]

Techniques used to identify DNA-binding sites and analyze protein−DNA interactions include electrophoretic mobility shift assays,[2,5−7] DNA−protein photo-cross-linking,[2] DNA−protein co-precipitation assays,[8] DNA footprinting,[2] fluorescence spectroscopy,[2] and atomic force microscopy.[9,10] Limitations of these methods include a lack of easily extractable quantitative information, inability to minimize effects of nonspecific interactions, difficulty in measuring weak interactions, perturbation in DNA binding caused by covalently attached probes, and failure in many cases to detect cooperative binding.[2,3]

Surface plasmon resonance (SPR) sensing techniques have been used to measure kinetics and equilibrium binding constants of protein−DNA interactions with high sensitivity without the need for labels.[11−27] Most of these studies have used SPR spectroscopy

* Corresponding author. Fax: 206-616-6250. E-mail: campbell@chem.washington.edu.

† University of Washington.

‡ Current address: Max-Planck-Institut für Polymerforschung, Ackermannweg 10, D-55128 Mainz, Germany.

§ Institute for Systems Biology.

(1) Pabo, C. O.; Sauer, R. T. *Annu. Rev. Biochem.* **1992**, *61*, 1053−1095.
(2) Guille, M. J.; Kneale, G. G. *Mol. Biotechnol.* **1997**, *8*, 35−52.
(3) Hard, T.; Lundback, T. *Biophys. Chem.* **1996**, *62*, 121−139.
(4) JenJacobson, L. *Biopolymers* **1997**, *44*, 153−180.
(5) Brenowitz, M.; Senear, D. F.; Shea, M. A.; Acker, G. K. *Methods Enzymol.* **1986**, *130*, 132−181.
(6) Yuh, C. H.; Ransick, A.; Martinez, P.; Britten, R. J.; Davidson, E. H. *Mech. Dev.* **1994**, *47*, 165−186.
(7) Galas, D.; Schmitz, A. *Nucleic Acids Res.* **1978**, *5*, 3157−3170.
(8) Franza, B. R.; Josephs, S. F.; Gilman, M. Z.; Ryan, W.; Clarkson, B. *Nature* **1987**, *330*, 391−395.
(9) Yokota, H.; Fung, K.; Trask, B. J.; van den Engh, G.; Sarikaya, M.; Aebersold, R. *Anal. Chem.* **1999**, *71*, 1663−1667.
(10) Pang, D.; Yoo, S.; Dynan, W. S.; Jung, M.; Dritschilo, A. *Cancer Res.* **1997**, *57*, 1412−1415.
(11) Bambdad, C. *Biophys. J.* **1998**, *75*, 1997−2003.
(12) Buckle, M.; Williams, R. M.; Negroni, M.; Buc, H. *Proc. Natl. Acad. Sci. U.S.A.* **1996**, *93*, 889−894.
(13) Kok, R. J.; D'Argenio, D. A.; Ornston, L. N. *J. Bacteriol.* **1998**, *180*, 5058−5069.
(14) van Leeuwen, H. C.; Strating, M. J.; Rensen, M.; deLaat, W.; vanderVliet, P. C. *EMBO J.* **1997**, *16*2043−2053.
(15) Malmborg, A. C.; Johansson, K.; Sigvardsson, M.; Borrebaeck, C. A. *Mol. Immunol.* **1995**, *32*, 1429−1442.
(16) Jakimowicz, D.; Majka, J.; Messer, W.; Speck, C.; Fernandez, M.; Martic, M. C.; Sanchez, J.; Schauwecker, F.; Keller, U.; Schremf, H. *Microbiology* **1998**, *144*, 1281−1290.
(17) Bondeson, K.; Rönn, O.; Magnusson, G. *FEBS Lett.* **1998**, *423*, 307−313.
(18) Fisher, R. J.; Rein, A.; Fivash, M.; Urbaneja, M. A.; Casas-Finet, J. R.; Madeaglia, M.; Henderson, L. E. *J. Virol.* **1998**, *72*, 1902−1909.

10.1021/ac035159j CCC: $27.50
Published on Web 03/04/2004

to measure interactions between wild-type (WT) and mutated proteins and their WT- and mutated DNA-binding regions. For these types of experiments, the dsDNAs containing the appropriate sequence for protein binding are immobilized on an SPR-active sensor, typically a commercially available dextran-coated surface.[12−25] Then DNA-binding protein in solution is introduced to the surface-immobilized dsDNAs, and real-time binding curves are measured by tracking the shift in the angle or wavelength at which the SPR of a thin metal film is optically excited as protein binds to the binding site in the dsDNA. Typically, the amount of protein bound to the dsDNAs is quantified by fitting the SPR curve (intensity versus incident angle) measured after adsorption to a bilayer model with Fresnel equations to determine both the average thickness (within the probed area) and the refractive index of the adsorbed film.[28−30] Alternatively, simple methods based on measuring the SPR instrument's sensitivity factor can be used to convert the changes in the SPR angle or wavelength into an effective refractive index change, an effective thickness, or an adsorbate surface concentration.[31]

One limitation of these SPR spectroscopy investigations is typically only one dsDNA sequence or protein can be studied at a time. Due to the number of experiments that would be required to investigate every possible mutation in a DNA-binding domain of a protein and in the base-pair sequence of the DNA-binding site, a high-throughput method for studying protein−DNA interactions is desirable. Additionally, recent reports of the nonadditivity of DNA-binding site mutations by two research groups underscores the need to develop a technique that provides quantitative information about the changes in the strength and specificity of protein−DNA interactions in a parallel, high-throughput manner.[32−35]

In this paper, we describe the development of such a high-throughput technique based on SPR microscopy that provides real-time adsorption and desorption information about protein binding to surface-immobilized dsDNAs arranged as an array on a planar sensor surface. Recently Corn and co-workers used SPR microscopy (also called "SPR imaging") to study protein−DNA interactions in a parallel fashion.[27,36] For these studies, an alternating array of dsDNAs containing a protein-binding sequence and other dsDNAs without this sequence was created on a gold-coated surface. Single-time-point measurements were used to obtain information about equilibrium binding of a protein to the dsDNA array. Line profiles of intensity images were used to compare relative amounts of adsorbed proteins on the dsDNA array elements.[27,36] Similar methods were used to study DNA−DNA[37−41] and RNA−DNA[41] interactions.

In an effort to obtain information about adsorption and desorption kinetics, we use SPR microscopy here to study adsorption and desorption processes in real time rather than at a single time point by measuring changes in reflected light intensity at a single "high contrast" angle selected from the linear region of the SPR curve (reflectivity versus angle) as described in ref 42. Additionally, we show here that the measured changes in reflected intensity at such an angle can be converted to absolute coverages of protein. These quantitative methods are described in more detail in ref 42 and are based on extending formulas used to quantitate SPR spectroscopy data (SPR angle and wavelength shifts) to changes in reflected intensity measured by SPR microscopy. Similar to methods used for quantitating SPR spectroscopy data,[31] these methods rely on a sensitivity factor for the SPR microscope based on simple measurements of the instrument's response to bulk changes in solution refractive index.[42]

We demonstrate the ability to measure quantitative, real-time adsorption and desorption kinetics in a highly parallel fashion by measuring the sequence-specific binding of the DNA-binding Gal4 protein to its binding site immobilized in an array on an SPR-active surface. Many groups have investigated the interactions between Gal4 and its binding operator to better understand the role of Gal4 as a regulatory protein for yeast gene expression.[1,25,43−53] The protein binds as a homodimer to a 17-base-pair dsDNA sequence (shown in Figure 1) containing the binding site for the protein.[48] The protein controls genes involved in galactose

(19) Yamamato, A.; Ando, Y.; Yoshioka, K.; Saito, K.; Tanabe, T.; Shirakawa, H.; Yoshida, M. *J. Biochem.* **1997**, *122*, 586−594.
(20) Gotoh, M.; Hasebe, M.; Ohira, T.; Hasegawa, Y.; Shinohara, Y.; Sota, H.; Nakao, J.; Tosu, M. *Genet. Anal.* **1997**, *14*, 47−50.
(21) Galio, L.; Briquet, S.; Cot, S.; Guillet, J. G.; Vaquero, C. *Anal. Biochem.* **1997**, *253*, 70−77.
(22) Haruki, M.; Noguchi, E.; Kanaya, S.; Crouch, R. J. *J. Biol. Chem.* **1997**, *272*, 22015−22022.
(23) Seimiya, M.; Kurosawa, Y. *FEBS Lett.* **1996**, *398*, 279−284.
(24) Pond, C. D.; Holden, J. A.; Schnabel, P. C.; Barrows, L. R. *Anti-Cancer Drugs* **1997**, *8*, 336−344.
(25) Wu, Y.; Reece, R. J.; Ptashne, M. *EMBO J.* **1996**, *15*, 3951−3963.
(26) Smith, E. A.; Erickson, M. G.; Ulijasz, A. T.; Weisblum, B.; Corn, R. M. *Langmuir* **2002**, *19*, 1486−1492.
(27) Brockman, J. M.; Frutos, A. G.; Corn, R. M. *J. Am. Chem. Soc.* **1999**, *121*, 8044−8051.
(28) Knoll, W. *Annu. Rev. Phys. Chem.* **1998**, *49*, 569−638.
(29) Homola, J.; Yee, S. S.; Gauglitz, G. *Sens. Actuators, B* **1999**, *54*, 3−15.
(30) Brockman, J. M.; Nelson, B. P.; Corn, R. M. *Annu. Rev. Phys. Chem.* **2000**, *51*, 41−63.
(31) Jung, L. S.; Campbell, C. T.; Chinowsky, T. M.; Mar, M. N.; Yee, S. S. *Langmuir* **1998**, *14*, 5636−5648.
(32) Bulyk, M. L.; Huang, X.; Choo, Y.; Church, G. M. *Proc. Natl. Acad. Sci. U.S.A* **2001**, *98*, 7158−7163.
(33) Man, T.-K.; Stormo, G. D. *Nucleic Acids Res.* **2001**, *15*, 2471−2478.
(34) Bulyk, M. L.; Johnson, P.; Church, G. M. *Nucleic Acids Res.* **2002**, *30*, 1255−1261.
(35) Benos, P. V.; Bulyk, M. L.; Stormo, G. D. *Nucleic Acids Res.* **2002**, *30*, 4442−4451.
(36) Frutos, A. G.; Brockman, J. M.; Corn, R. M. *Langmuir* **2000**, *16*, 2192−2197.
(37) Li, M.; Lee, H. J.; Condon, A. E.; Corn, R. M. *Langmuir* **2002**, *18*, 805−812.
(38) Thiel, A. J.; Frutos, A. G.; Jordan, C. E.; Corn, R. M.; Smith, L. M. *Anal. Chem.* **1997**, *69*, 4948−4956.
(39) Jordan, C. E.; Corn, R. M. *Anal. Chem.* **1997**, *69*, 1449−1456.
(40) Nelson, B. P.; Frutos, A. G.; Brockman, J. M.; Corn, R. M. *Anal. Chem.* **1999**, *71*, 3928−3934.
(41) Nelson, B. P.; Grimsrud, T. E.; Liles, M. R.; Goodman, R. M.; Corn, R. M. *Anal. Chem.* **2001**, *73*, 1−7.
(42) Shumaker-Parry, J. S.; Campbell, C. T. *Anal. Chem.* **2004**, *76*, 907−917.
(43) Baleja, J. D.; Thanabal, V.; Wagner, G. *J. Biomol. NMR* **1997**, *10*, 397−401.
(44) Corton, J. C.; Moreno, E.; Johnston, S. A. *J. Biol. Chem.* **1998**, *273*, 13776−13780.
(45) Corton, J. C.; Johnston, S. A. *Nature* **1989**, *340*, 724−727.
(46) Giniger, E.; Varnum, S. M.; Ptashne, M. *Cell* **1985**, *40*, 767−774.
(47) Lohr, D.; Venkov, P.; Zlatanova, J. *FASEB J.* **1995**, *9*, 777−787.
(48) Marmorstein, R.; Carey, M.; Ptashne, M.; Harrison, S. C. *Nature* **1992**, *356*, 408−414.
(49) Melcher, K.; Xu, H. E. *EMBO J.* **2001**, *20*, 841−851.
(50) Parthum, M. R.; Jaehning, J. A. *J. Biol. Chem.* **1990**, *265*, 209−213.
(51) Sadowski, I. In *Genetic Engineering: Principals and Methods*; Setlow, J. K., Ed.; Plenum Press: New York, 1995; Vol. 17, p 119.
(52) Vashee, S.; Xu, H.; Johnston, S. A.; Kodadek, T. *J. Biol. Chem.* **1993**, *268*, 24699−24706.
(53) Johnston, M. *Microbiol. Rev.* **1987**, *51*, 458−467.

Figure 1. Gal4 dsDNA operator (i.e., the dsDNA sequence which forms the binding site for the Gal4 protein as a homodimer). The gray boxes highlight the fact that the base pair sequence is palindromic.

metabolism by binding to this palindromic site in the presence of galactose and activates transcription of several other transcription factors.[46] Studies of these Gal4−DNA interactions have increased the current understanding of eukaryotic gene regulation.[1]

For the study presented in this paper, we immobilized dsDNAs on a sensor surface using a streptavidin (SA) linker layer on a BAT/OEG SAM-functionalized gold-coated surface. This SA layer provides a high density of biotin-binding sites for immobilization of biotinylated dsDNA, while maintaining a minimum spacing between the dsDNAs.[54,55] The sequences of the two dsDNAs used for our Gal4-binding experiments are shown in Table 1. One sequence, which we will call the "operator", contains the binding site sequence that selectively binds Gal4. The other dsDNA does not have this sequence and serves as the "control". The biotinylated dsDNA sequence attached to the 5′ end of the operator acts as a spacer between the Gal4-binding site and the sensor surface to minimize the impact the surface might have on the protein−DNA interactions. The biotin is attached to the dsDNA through a 12-carbon linker (Figure 2) that provides flexibility and spacing so that its biotin tail group can fit into its binding pocket in the SA. This functionality is designated as BiotinX in Table 1. The lengths of the DNAs (100 base pairs and 77 base pairs) were selected to help control the minimal spacing between the dsDNAs to allow space for the protein homodimer complex to bind to them. In earlier studies, we observed that the length of the dsDNAs controls the packing density of biotinylated dsDNAs immobilized on an SA monolayer formed on a BAT/OEG-functionalized gold-coated sensor surface.[56] For example, when dsDNAs containing 107 base pairs were immobilized on a SA-functionalized surface, a packing density of 9.7×10^{11} dsDNA/cm^2 was obtained. This packing density for the 107-base-pair dsDNA corresponds to a binding ratio of 0.44 dsDNA/SA, However, the saturation coverage of a shorter dsDNA (24 base pairs) was 2.8×10^{12} DNA/cm^2 for a SA surface prepared in the same way, or 1.3 dsDNA per surface streptavidin, much closer to the stoichiometric ratio of 2. This packing density dependence on the dsDNA length is probably due to electrostatic repulsions between the negatively charged molecules that behave as rigid rods[57] at these lengths rather than the excluded volume of the polymer molecule.[58] The packing density of the 107-base-pair dsDNA leads to an average spacing between dsDNAs of ∼10 nm, assuming a square lattice for the SA molecules. This spacing should be adequate to allow the formation of the Gal4 homodimer, while still providing an adequate density of binding sites for sensitive detection of binding events.

Microarrays containing negative control and operator dsDNAs were fabricated using a commercial robotic microspotting system that uses a pin to deliver a few nanoliters of solution to a specified location on the sensor surface to create a dsDNA-containing array element. The microspotting process and the fabrication and characterization of dsDNA arrays created using a SA linker layer are described in more detail in ref 55. For the studies described here, we use those same techniques to fabricate a 10×12 array of 200-μm-diameter elements containing the operator and control dsDNAs with an average packing density within each element of $\sim 7 \times 10^{11}$ dsDNA/cm^2, or a binding ratio of ∼0.4 dsDNA/SA. Each array element (control and operator) was repeated numerous times on the sensor surface, and the SPR microscope was used to measure individual adsorption curves in real time for each element simultaneously. We show here that the SPR response measured at a control sequence element can be used to correct the SPR response measured simultaneously at an operator sequence for common reflected intensity changes due to noise, bulk refractive index changes, and nonspecific adsorption. The corrected SPR reflectivity (at a high contrast angle) measured with the video camera provides real-time adsorption and desorption curves for specific protein binding to its dsDNA-binding site immobilized on the sensor surface. We demonstrate a real-time protein adsorption detection limit of ∼0.5 pg of protein in a 200-μm dsDNA spot on the surface with 1-s time resolution. Only two different dsDNAs are used in the proof-of-principle experiments presented in this paper. However, we show with this 120-element array that one could use the same experimental methods to investigate protein adsorption at >100 different dsDNA sequences immobilized on the sensor surface in parallel, thus providing a method for high-throughput analysis of DNA-binding proteins or protein−dsDNA interactions.

EXPERIMENTAL SECTION

Substrate and SAM Preparation. Gold-coated substrates were prepared by cleaning $25 \times 35 \times 3$ mm SF14 glass slides (Schott Glass Technology, Durea, PA) by sonication in 2% RBS-35 detergent (VWR International) solution in distilled water at 50 °C for 30 min. The slides were rinsed by sonication in distilled water three times, rinsed with absolute ethanol, and dried with N_2 before being placed in an oven at 100 °C for 45 min. The slides were coated with 20 Å of chromium followed by 475 Å of gold by electron beam evaporation. The gold-coated substrates were used immediately or stored under N_2. Immediately before surface functionalization, the gold-coated substrates were cleaned by immersing them in a basic peroxide solution (15% ammonium hydroxide, 15% hydrogen peroxide, 70% water) at 65 °C for up 1 min. The slides were rinsed copiously with Nanopure water (18 MΩ resistivity), rinsed with absolute ethanol, and dried with N_2.

Oligo(ethylene glycol)-terminated thiol (OEG) was synthesized by Dr. Esmaeel Naeemi and provided by Prof. Buddy Ratner (University of Washington). Biotin-terminated thiol (BAT) was synthesized by Dr. Maximilliane Boeckl and provided by Prof. Tomikazu Sasaki (University of Washington). These molecules are described in detail elsewhere.[59] The clean, gold-coated substrates were immersed in a jar containing a deoxygenated

(54) Shumaker-Parry, J. S.; Campbell, C. T.; Stormo, G. D.; Silbaq, F. S.; Aebersold, R. H. *Proc. SPIE-Scanning and Force Microscopies for Biomedical Applications II*; SPIE: San Jose, CA, 2000; pp 158−166.
(55) Shumaker-Parry, J. S.; Zareie, M. H.; Aebersold, R. H.; Campbell, C. T. *Anal. Chem.* **2004**, *76*, 918−929.
(56) Xia, N.; Shumaker-Parry, J. S.; Zareie, M. H.; Campbell, C. T.; Castner, D. G. *Langmuir*, in press.
(57) Hagerman, P. J. *Annu. Rev. Biophys. Biophys. Chem.* **1988**, *17*, 265−286.
(58) Delrow, J. W.; Gebe, J. A.; Schurr, J. M. *Biopolymers* **1997**, *42*, 455−470.
(59) Nelson, K. E.; Gamble, L.; Jung, L. S.; Boeckl, M. S.; Naeemi, E.; Golledge, S. L.; Sasaki, T.; Castner, D. G.; Campbell, C. T.; Stayton, P. S. *Langmuir* **2001**, *17*, 2807−2816.

Table 1. Operator and Control DNA Sequences Used for Gal4 Binding Studies[a]

	Operator dsDNA
Gal4 operator	5'-CGGAGGACAGTCCTCCG-3'
sequence attached to 5' end of operator	5'-BiotinX-GAGGAGACGACGCAATTAGTACGACGTGTAGTCCCA TCATGAGTGCTCGACATGATGTTACGCTGCTACTAGTAG-3'
sequence attached to 3' end of operator	5'-TACGACGT-3'
	Control dsDNA
control sequence	5'-BiotinX-GGCAATTAACCCTCACTAAAGGGAACAAAATGCTCG AGGTCGACGGTATCGCGTGGGCGCTCGAGGTCGACGGTATC-3'

[a] The dsDNAs formed by hybridization of the oligonucleotides shown in the table with their complementary sequences were immobilized in an array on an SPR-active surface.

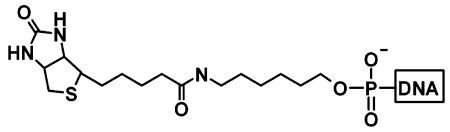

Figure 2. Bond-line structure of biotinX, the biotin-terminated functionality covalently attached to the 5′ end of one strand of the dsDNA for immobilization via a streptavidin linker layer.

solution of absolute ethanol containing BAT and OEG (1:9 mole ratio of BAT and OEG, respectively). The jar was purged with N_2 and placed in a dark location for 12−24 h to allow the thiols to assemble on the surface. The substrates were removed from solution, rinsed liberally with absolute ethanol to remove loosely bound thiols, and dried with N_2. This procedure was shown previously to produce a self-assembled monolayer on the gold surface with a BAT/OEG ratio in the SAM of ∼0.3,[59] which is optimal for binding a SA monolayer.[59,60] Slides that were not used immediately were placed in a covered Petri dish filled with N_2 and sealed with Parafilm. The Petri dish was placed in a larger jar purged with N_2 and sealed with Parafilm for long-term storage.

dsDNA Solution Preparation. Biotinylated DNAs were prepared from single-stranded oligonucleotides synthesized by Integrated DNA Technologies (Coralville, IA). For two complementary ss-oligos, one strand contains a 5′-biotin modification (shown in Table 1) and the other strand has no modification. To prepare dsDNAs, complementary ss-oligos (stored in 10 mM Tris, 10 mM NaCl, 1 mM EDTA in Nanopure water) were combined in equimolar ratios in an Eppendorf tube and placed in boiling water that was allowed to cool slowly to room temperature. The dsDNAs were stored at −20 °C. The dsDNAs were thawed and used to prepare the dsDNA microspotting solutions (7.0 or 3.5 μM) in 0.4 or 1.0 M phosphate-buffered saline (PBS) at pH 7.4.

Streptavidin and Albumin Solutions. Streptavidin was purchased from Calbiochem (San Diego, CA) and used without further purification. SA solution for microspotting was prepared at a concentration of 0.14 mg/mL in 150 mM PBS buffer at pH 7.4. The same buffer was used to prepare SA solution (0.06 mg/mL) for adsorption to the SPR microscope sensor surface. Bovine serum albumin (BSA) solution was prepared as 1.0 mg/mL BSA in the running buffer (30 mM Tris at pH 8.0, 50 mM NaCl, 3 mM dithiothreitol (DTT), 20 μM $ZnSO_4$).

Gal4 Protein Solution. Purified solutions of Gal4 protein (amino acids 1−147, molecular weight ∼20 000) was provided by Prof. Ivan Sadowski (University of British Columbia, Vancouver, BC, Canada). The protein has a 6-histidine tag for easier purification and contains the domains responsible for site-specific dsDNA binding and homodimer formation.[61] Stock solutions of the protein were stored at −20 °C in storage buffer (50 mM PBS at pH 7.4, 5 mM $MgCl_2$, 10 μM $ZnSO_4$, 0.5 mM DTT). Prior to adsorption experiments, the Gal4 stock solutions were thawed and diluted to the desired concentration in the running buffer.

Microspotting Procedures. Robotic Arraying System. The microspotting apparatus and procedure used to make the dsDNA array is described in detail in ref 55. Briefly, a ChipWriter Pro robotic arraying system (Virtek Biotech, Waterloo, Canada) was used with a Stealth printhead and ArrayIt microspotting pins (TeleChem, International, Inc., Sunnyvale, CA). The robot controls the motion of the printhead that holds microspotting pins that each deliver a droplet containing a few nanoliters of sample to the substrate surface in preselected sites on the surface. Here, we used only a single pin (SMP7, TeleChem International, Inc.). This pin has a sample uptake volume of 250 nL and an estimated delivery volume of 1.7 nL to create a spot of ∼200-μm diameter.[62]

Prior to microspotting, 8−10 μL of SA solution or dsDNA solution was transferred to the appropriate wells in a 384-well microtiter plate (Uniplate, 7701-5101, Whatman, Clifton, NJ), which was transferred to the platform in the microspotting chamber, and controlled to 75% relative humidity and ∼24.5 °C. The robot was programmed to clean and fill the pin and deposit multiple sample droplets in a row on a single substrate to minimize sample volume requirements and shorten the microarray fabrication time. The pin was cleaned and filled with new sample for each row. The center-to-center spot spacing is 450 μm.

The SA arrays were made by first spotting SA solution (0.14 mg/mL) onto a gold-coated substrate functionalized with the BAT/OEG mixed monolayer. The protein was allowed to adsorb from the nanoliter droplets in the high-humidity chamber for 30 min. Then dsDNA solution (7.0 or 3.5 μM) in 0.4 or 1.0 M PBS buffer, pH 7.4, was spotted on top of the SA spots. The substrate was kept in the high-humidity chamber for 30 min before it was rinsed and stored in PBS buffer at 4 °C until analysis. Longer

(60) Jung, L. S.; Nelson, K. E.; Stayton, P. S.; Campbell, C. T. *Langmuir* **2000**, *16*, 9421−9432.

(61) Sadowski, I.; Ptashne, M. *Nucleic Acids Res.* **1989**, *17*, 7539−7539.

(62) TeleChem International, http://www.arrayit.com.

adsorption times did not lead to higher coverages of SA or dsDNA.

SPR Microscopy Image Capture and Analysis. The arrays were characterized using our home-built SPR microscope described and characterized elsewhere.[42,63] Briefly, a stabilized 632.8-nm HeNe laser is p-polarized, expanded, and collimated before traveling through an SF14 glass hemicylindrical prism and substrate to illuminate an ~24-mm^2 area of a gold-coated sensor surface. The reflected light is focused and directed by a lens directly onto the CCD detector of a video camera, creating an image that is automatically digitized by a framegrabber card (DT3155, Data Translation, Marlboro, MA) and stored using image acquisition software (KSA400, k-Space Associates, Inc., Ann Arbor, MI). The software controls the CCD camera exposure time, frame averaging, and conversion of measured light intensity values to gray scale levels. The detection optics are connected to an aluminum rail that is attached to a motorized rotation stage. This stage is mounted under an identical stage that holds the prism. The centers of rotation for the two stages are aligned. A computer connected to a stage controller/driver is used to separately and equally vary the angle of incidence and the angle of detection so the CCD detector stays at the specular angle for each angle of incidence. A neutral density filter decreases the laser power to prevent saturation of the CCD detector. The entire system is mounted on a laser table and covered by a black box to minimize stray light, dust, and air flow effects.

The fluidics system includes a low-volume (~15 μL) flow cell, a syringe pump, two switching valves, and low dead-volume laminar flow tubing. The syringe is computer controlled using existing software for rapid time-response injection (~1 s).

Prior to SPR analysis, the substrate functionalized with the microarray was removed from the storage buffer and the back of the substrate was rinsed with water and blown dry with N_2. Then index match solution (Cargille Laboratories, Inc.) was applied to the back of the substrate and it was mounted on the SPR prism. The flow cell was mounted on the face of the substrate/prism assembly and filled with running buffer. All of these steps were done quickly to minimize exposure of the microarray to dry laboratory air.

The KSA 400 software provided several modes of collecting reflectivity data from the CCD video camera, including single-image capture, multiple image movie acquisition, and a special scan mode. Scan mode allows area integration of the intensity in an unlimited number of preselected regions of an SPR microscope image, and the integrated intensity for each selected region can be plotted versus time in real time with time resolution of 1/15 of 1 s. This mode was used to collect SPR curves (percent reflected intensity versus angle) and to monitor adsorption and desorption in real time simultaneously on each element of the array. Signal averaging over preselected time windows can also be performed for each area.

All SPR microscope images were collected at a high contrast angle in the linear region of the SPR curve for the array elements or, when possible, at an angle in the linear region for both the array elements and the surrounding surface.[42,55] For data acquisition using scan mode, 12 pixels × 18 pixel areas of the image were selected by placing a box on a preselected region of the image. Due to the incident angle, the horizontal magnification in the image is compressed by a factor of 1/cos Θ, where Θ is the incident angle. Thus, the box size corresponds to an approximately 200 μm × 200 μm area of the sensor surface. The video camera acquires 30 frames/s, but frames were averaged for 1 s by the computer for all data reported here, which sets the time resolution at 1 s. To measure SPR curves for all regions of interest, the reflected light intensity collected by the CCD video camera was area-integrated and averaged for the pixels within the preselected areas as the incident/detection angles were scanned (simultaneously, so that the detection angle was always at the specular angle). For visual clarity, the contrast and brightness was adjusted for SPR microscope images. However, all SPR curves, line scans, and adsorption/desorption curves presented here are composed of unfiltered intensity data or were made using unfiltered images.

SPR Microscopy Data Quantitation. The reflected intensity shifts monitored by the SPR microscope were converted to changes in the effective refractive index of the probe volume (η_{eff}) and then into effective adlayer thicknesses and absolute adsorbate coverages (e.g., the mass of bound protein per unit area) using the method for quantitation of SPR microscopy data described in detail in ref 42. (The effective adlayer thickness is defined as the thickness that the same amount of adsorbate per unit area would have if packed at its bulk density without any trapped solvent in the adlayer.) The foundation for these methods comes from quantitation of SPR spectroscopy data described previously.[31] Quantitation involves a sensitivity calibration based on the instrument's response to changes in bulk index of refraction of solutions, an exponential probe depth estimated from Fresnel equations, and the known index of refraction for the adsorbate. The index of refraction used for proteins (SA and Gal4) is 1.57[31] and that for DNA is 1.7.[64,65] A value for the system sensitivity (*s*) of 3900% reflected intensity per refractive index unit (RIU) was measured. A specific volume of 0.77 cm^3/g was used for SA and Gal4.[31] A density of 1.7 g/cm^3 was used for dsDNA, derived from its partial molar volume in aqueous solution.[66] A decay length of 234 nm was calculated for the excitation wavelength of 633 nm using previously described methods.[31]

RESULTS

dsDNA Array Characterization. A dsDNA was fabricated for Gal4 adsorption studies on a BAT/OEG SAM-functionalized gold-coated substrate using a SA linker layer as described in detail in ref 55. First, a SA array was made by spotting solution containing SA in a 10 × 12 array on a gold surface prefunctionalized with a BAT/OEG mixed monolayer. Then dsDNA in PBS buffer, pH 7.4, was spotted on top of the SA spots. Figure 3 shows SPR reflectivity versus angle curves for three different regions of the array in contact with 150 mM PBS buffer at pH 7.4. These curves were measured using scan mode to integrate the reflected intensity for preselected 200 μm × 200 μm regions of the sensing surface at a rate of 30 Hz while the incident angle was scanned. The curves are representative of curves measured for regions of the same size and with the same composition across the array. Each data

(63) Shumaker-Parry, J. S.; Nelson, K. E.; Aebersold, R. H.; Campbell, C. T., In preparation.

(64) Harrington, R. E. *J. Am. Chem. Soc.* **1970**, *92*, 6957−6964.

(65) Wu, P. G.; Fujimoto, B. S.; Song, L.; Schurr, J. M. *Biophys. Chem.* **1991**, *41*, 217−236.

(66) Darnell, J. E.; Lodish, H.; Baltimore, D. *Molecular Cell Biology*; Scientific American Books: New York, 1990.

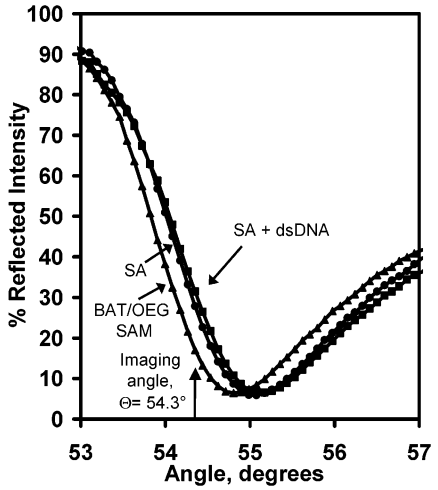

Figure 3. Representative reflectivity versus angle curves for the dsDNA array fabricated on a SA array formed on a preadsorbed BAT/OEG SAM. The curves were measured for three 0.04-mm^2 regions of the array shown in Figure 4 while the incident angle was scanned with the array under buffer. Each data point is the area-integrated intensity in the selected region averaged for 1 s (during which 30 video frames are collected). The curves were used to select a high-contrast angle for further SPR microscopy measurements.

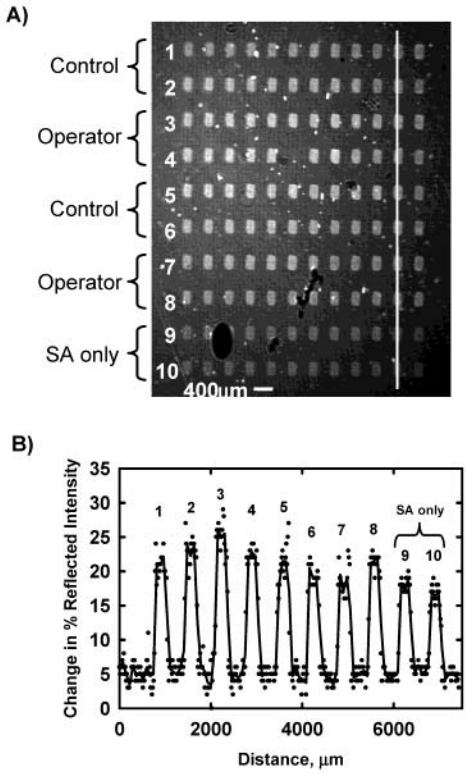

Figure 4. SPR microscope image and line profile of a dsDNA array under buffer solution. (A) The dsDNA array was fabricated on a SA array on a BAT/OEG SAM-functionalized gold-coated substrate. The image was collected at the high-contrast angle shown in Figure 3. The dsDNA and NaCl concentrations used for spotting each row are shown in Table 2. (B) The profile is an average of the line profile for a 4-pixel-wide (67 μm) column centered on the line shown in (A). The solid curves in all line profiles are five-point smoothed versions of these data. All images are the result of averaging frames collected by the CCD camera at a rate of 30 Hz for 1 s.

point is an average of 1 s of measurements, with an angle scan rate of ~0.1 deg/s. As expected, the curves for regions containing SA (circles) and SA/dsDNA (squares) are shifted to higher angles compared to the curve measured for the region that should contain only the BAT/OEG SAM (triangles), due to their higher effective refractive index (η_{eff}). Also, the SPR curve for the spots of dsDNA on SA is shifted to higher angles than that for the spots that should contain only SA. Although the reflectivity versus angle curves are offset from each other, we were able to select a single high-contrast incident angle that falls in the linear region for all three curves (i.e., for all three types of surfaces). This allows simultaneous measurement and quantitation of reflected intensity data for all areas of the surface.

The high-contrast angle (54.3°) shown in Figure 3 was used to collect the SPR microscope image of the dsDNA array shown in Figure 4A. The 10 × 12 array consists of rows containing dsDNA with the binding site for Gal4 (operator) and dsDNAs without this binding site (control). The bottom two rows of the array contain SA spots without dsDNA. The reflectivity curves show why there is contrast in the SPR microscope image in Figure 4A. The contrast comes from the heterogeneity in the complex dielectric constant due to differences in the effective refractive index (η_{eff}) or thickness (t) of the adsorbed layer on or near the sensing surface. Regions of the array where the effective refractive index satisfies the resonance condition at the imaging/detection angle used will appear almost completely dark, as the light is coupled efficiently into the surface plasmon excitations. Regions with the η_{eff} far from resonance will exhibit nearly 100% reflectivity and appear very bright. Regions where η_{eff} is close to the resonance value will be of "high contrast", showing strong and nearly linear dependence of light intensity on η_{eff}.[42] At the high-contrast imaging angle, the dsDNA and SA array spots in the SPR microscope image in Figure 4A appear bright compared to the surrounding surface because of the higher reflected intensity at these areas of the surface for the imaging angle as shown by the SPR curves. The increased reflected intensity is a result of the shift in the SPR curve for the elements due to the adsorbed SA and dsDNA layers compared to the BAT/OEG SAM. The high contrast between the spots and the surrounding surface makes it easy to identify the spots and their boundaries. Although different dsDNA and NaCl concentrations were used for microspotting, the intensities of the dsDNA spots appear similar for all dsDNA array rows. As expected, the reflected light intensity for the SA spots is slightly lower than that for the spots composed of SA plus dsDNA.

These qualitative intensity observations are verified by the line profile in Figure 4B and the data in Table 2. The profile is for the line shown in the SPR microscope image in Figure 4A. The reflected intensity values plotted in the profile are from a single video image (time-averaged for 1 s) and represent an area (line) average of the intensity values for a 67-μm-wide column centered on the column of array elements indicated by the line in Figure 4A. The reflected intensity data (dotted line) and the data smoothed by averaging a data point at the smoothing location with the two closest neighboring data points on each side (solid line) are shown in the profile. The profile of the line shows that the dsDNA spot intensities are similar and the intensity of the spots containing only SA is less than the spots composed of SA and dsDNA as observed in the images.

Table 2. Coverage of dsDNA and SA in an Array Created Using the Robotic Microarraying System

row no.	spotting solution conditions, [DNA], [NaCl]	diff in % reflected intensity[a]	SD (% reflected intensity)	diff in % reflected intensity due to dsDNAs[b]	effective thickness (nm)	surface density (10^{12} molecule/cm^2)	binding ratio (dsDNA/streptavidin)[c]
1	7.0 μm, 0.4 M	16.6	1.7	4.0	0.34	0.71	0.34
2	7.0 μm, 1.0 M	16.8	1.4	4.2	0.35	0.72	0.34
3	7.0 μm, 0.4 M	18.4	1.8	5.8	0.48	0.77	0.36
4	7.0 μm, 1.0 M	18.6	0.9	6.0	0.49	0.79	0.38
5	3.5 μm, 0.4 M	18.3	1.6	5.7	0.46	0.96	0.46
6	3.5 μm, 1.0 M	17.4	1.3	4.8	0.40	0.82	0.39
7	3.5 μm, 0.4 M	17.8	1.8	5.2	0.51	0.82	0.39
8	3.5 μm, 1.0 M	16.0	1.7	3.4	0.43	0.69	0.33
9	SA only	13.0	1.4		1.65	2.2	
10	SA only	12.2	1.5		1.55	2.0	

[a] Values for percent reflected intensity were found by using scan mode to integrate the light intensity in a 200 μm $\times$ 200 μm region in each array element and a region below the array element for the array shown in Figure 4. Differences in reflected intensity were found by subtracting the intensity for the surrounding region from that for the array spot and averaging for that row. Column 4 shows their spot-to-spot standard deviations (SD). [b] The differences in percent reflected intensity due to dsDNAs were found by subtracting the average percent reflected intensity for the rows containing SA from the rows containing SA plus DNA. [c] A SA packing density of 2.1×10^{12} SAs/cm^2 was used to estimate the binding ratios.

Table 2 presents a more comprehensive quantitative analysis of the SA and dsDNA spots. To obtain the reflected intensity values, scan mode was used to integrate the reflected intensity for a 200 μm $\times$ 200 μm area in the center of each element of the array and in the same size area of the BAT/OEG surface located just below each array element. The difference in reflected intensity was calculated by subtracting the intensity for the surrounding BAT/OEG surface from that for the array element. The differences in percent reflected intensity were averaged for each row and used to calculate the SA and dsDNA packing densities. The quantitative methods described in ref 42 were used to convert the intensity values to adsorbed layer thicknesses and SA and dsDNA surface coverages.

The quantitative data in Table 2 verify the qualitative observations. The differences in percent reflected intensity for the dsDNA spots range from 16.0 to 18.3% and convert to dsDNA surface densities ranging from 0.69×10^{12} to 0.96×10^{12} dsDNA/cm^2. The packing densities for all of the dsDNA array elements, regardless of the dsDNA length, dsDNA solution concentration, or salt concentration were similar to each other. This was expected from the uniformity in the intensity observed for the array elements in the SPR microscope images in Figure 4A and the line profile in Figure 4B.

Also, as shown by the SPR microscope image in Figure 4A and the line profile in Figure 4B, the differences in reflected intensity for the SA spots were lower than those for the spots containing SA and dsDNA. The average difference in reflected intensity for the SA spots in the two rows at the bottom of the array was 12.5%, corresponding to an average SA packing density of 2.1×10^{12} SA/cm^2 or 84% of the typical SA saturation coverage on these SAMs.[41,54,67] This average SA surface coverage was used to convert the calculated dsDNA coverages to the binding ratios shown in Table 2. The dsDNA/SA binding ratios range from 0.34 to 0.46 dsDNA/SA and are similar to the saturation binding ratio (0.44 dsDNA/SA) measured for similar length dsDNA adsorbed from bulk solution (as opposed to the solution droplets used here) onto a uniform SA monolayer immobilized on the same composition BAT/OEG SAM on gold.[54] We will show in the following sections that this packing density provides a high density of binding sites for detection of DNA-binding proteins, while allowing adequate space for protein binding.

Surface Preparation Prior to Gal4-Binding Experiments. The dsDNA array characterized in the previous section was used for Gal4 adsorption experiments. Prior to adsorbing the Gal4, the surface was modified by adsorbing SA from 150 mM PBS at pH 7.4 to fill in the areas between the array elements. The amount of SA adsorbed was estimated from binding curves collected for regions of the surface using scan mode. The average change in reflected intensity for 12 spatially separated regions of the BAT/OEG surface was 8.7 $\pm$ 1.2%. This converts to an effective SA layer thickness of 1.1 nm, or a SA packing density of 1.5×10^{12} SA/cm^2.

Although nonspecific binding of the protein Mnt onto SA-functionalized surfaces was minimal,[54] preliminary SPR spectroscopy experiments showed Gal4 does adsorb nonspecifically to surfaces functionalized with the BAT/OEG SAM or a SA monolayer. In an attempt to minimize nonspecific binding of Gal4 to the SA-functionalized areas of the array, we adsorbed BSA to try to passivate the surface. Prior to BSA adsorption, the running buffer was switched from the PBS buffer used for SA adsorption to the buffer that will be used for Gal4 adsorption (30 mM Tris at pH 8.0, 50 mM NaCl, 3 mM DTT, 20 μM $ZnSO_4$). The former will be referred to as the running buffer for the remainder of this paper.

When we first introduced BSA (0.1 mg/mL) in the running buffer to the surface, a small amount of BSA adsorbed to all areas of the sensing surface. This was observed by measuring an increase in reflected intensity in preselected areas of the surface using scan mode. The average percent reflected intensity increase for seven spatially separated areas, including areas with just SA and areas with dsDNA, was 0.52 $\pm$ 0.06. This converts to an effective BSA layer thickness of 0.07 nm or a surface coverage of 8.6×10^{10} BSA/cm^2. This BSA coverage is less than 5% of the BSA packing density of 1.82×10^{12} molecules/cm^2 measured for a bare gold surface using the SPR microscope[42] and measured previously using SPR spectroscopy.[31] A second injection of BSA

(67) Jung, L. S.; Nelson, K. E.; Campbell, C. T.; Stayton, P. S.; Yee, S. S.; Perez-Luna, V.; Lopez, G. P. *Sens. Actuators, B* **1999**, *54*, 137−144.

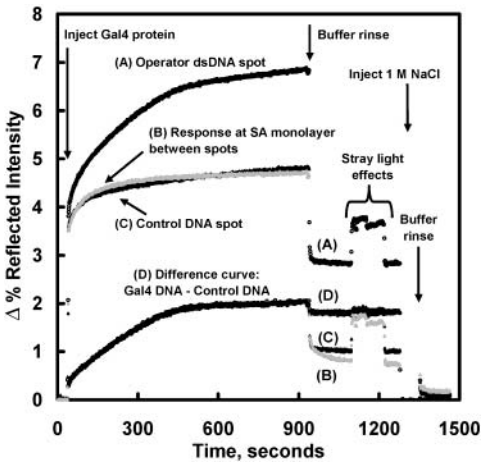

Figure 5. Representative real-time Gal4 adsorption and desorption curves measured for an operator dsDNA spot, a control dsDNA spot, and a region of the SA monolayer between the array elements. Before Gal4 injection, the surface was in buffer. The curves were collected by integrating the reflected intensity for 200 μm × 200 μm regions of the indicated surface areas during the introduction of various solutions to the sensor surface. Each data point is a 1-s average of intensities from video frames collected at a rate of 30 Hz. Difference curve shows how a control site (reference area) on the microarray surface can be used to compensate for reflected intensity changes due to noise, bulk refractive index changes, and nonspecific adsorption. The difference curve is the result of subtracting the response at the control dsDNA spot from the response measured for the operator dsDNA spot. The reflected intensity changes common to the control and operator curves are eliminated, including the noise due to stray light that reached the CCD camera when the box enclosing the microscope was opened to introduce a new sample solution. The response in the difference curve should be due to specific binding of Gal4 to the operator dsDNA spot. (The difference signal of 0% *during* the actual NaCl rinse is meaningless, since the intensity was saturated for both curves during that period.)

(0.1 mg/mL) led to an increase in the percent reflected intensity of 0.10 ± 0.02 for the same areas. The intensity increase for a third injection of the same concentration BSA solution produced a response of 0.05 ± 0.01% reflected intensity, ~10 times less than the response after the initial injection. After this third injection, the nonspecific BSA adsorption to the surface was assumed to be at saturation.

Real-Time Measurement of Gal4 Binding. (1) Gal4 Adsorption to the dsDNA Array. After SA adsorption and BSA adsorption, the array surface characterized above was used to measure the SPR microscope response for the adsorption of Gal4 onto the dsDNA array. SPR microscope images and binding curves were collected simultaneously during the adsorption experiment. From the video camera output frames (intensity versus position stored by the computer every second), curves of percent reflected light intensity versus time were generated with the computer for preselected areas within the illuminated region of the sensor surface using scan mode. (The computer was programmed to average the intensity over these areas and over a time period of 1 s.) Three representative response curves for regions of the surface containing the operator dsDNA, the negative control dsDNA, and the surrounding SA monolayer are shown in Figure 5.

Initially, the baseline was established with the array surface in contact with running buffer. Upon injection of Gal4 (0.125 mg/mL) solution, the reflected intensity increased rapidly for all three curves. The slope in the curve for the operator dsDNA is indicative of adsorption of the protein onto the sensor surface. However, the very rapid initial increase in reflected intensity for all three curves may be due to nonspecific protein adsorption or a higher bulk refractive index for the Gal4 solution compared to the running buffer due to differences in concentrations or temperature. (Below, we correct for the latter effects by comparison to control areas.) After adsorption slowed, the sensor surface was rinsed by replacing the Gal4 solution with the original, pure running buffer. Upon re-injection of the running buffer, the reflected intensity at the SA-only spots and at the control DNA spots decreased to ~1/7 of its maximum value and stabilized at an intensity level of ~0.6% absolute reflected intensity above the original baseline. This reflected intensity increase above the baseline indicates that there was a small amount of Gal4 adsorption onto the SA-only and control DNA surfaces. The intensity in the operator regions remained much higher, stabilizing at ~3% absolute reflected intensity. This is attributed to *specific* binding of Gal4 to the dsDNA operator sequence. The average response due to nonspecific Gal4 adsorption on regions surrounding the dsDNA array spots was 0.7 ± 0.1% reflected intensity. This converts to a nonspecific adsorption coverage of 3.6×10^{11} Gal4 proteins/cm^2. The Gal4 coverage on the operator and control dsDNA spots is discussed in more detail below.

Returning to the response to Gal4 injections, the reflected intensity increased more for the operator dsDNA spot compared to the other curves measured for the control dsDNA spots and the SA monolayer. This higher intensity increase for the operator dsDNA spot also is shown by the SPR microscope difference image in Figure 6. The difference image is the result of subtracting the intensities of an image of the array just prior to Gal4 injection from those at the same pixels of an image collected ~18 min after rinsing the Gal4-dosed surface with buffer. All of the array spots containing the operator dsDNA are visible in the image due to higher increases in the reflected intensity for these spots compared to the SA monolayer and the control dsDNA spots. Like the real-time adsorption curves, this shows that much more Gal4 binds to the operator dsDNA elements than to the control dsDNA or SA elements. The profile of the line shown in the SPR microscope image is plotted in Figure 6B. The reflected intensity values plotted in the profile are an average of the values for a 67-μm-wide column through the center of the array elements indicated by the line. The reflected intensity data (dotted line) and the smoothed data are shown in the profile. The profile shows a larger intensity difference for the operator dsDNA spots indicating a higher amount of Gal4 adsorption as compared to the control dsDNA spots and the surrounding region. The small reflected intensity difference for the control dsDNA spots indicates a small amount of nonspecific adsorption and a higher amount than on the surrounding region as shown by the real time binding curves in Figure 5.

The image in Figure 6A was used to quantitate the amount of Gal4 adsorption to the operator and control dsDNA spots by finding the difference in reflected intensity for a 200 μm × 200 μm area in the center of each control and operator dsDNA spot and the same size area just below that array element. The resulting values indicate the difference in the amount of Gal4 that adsorbed

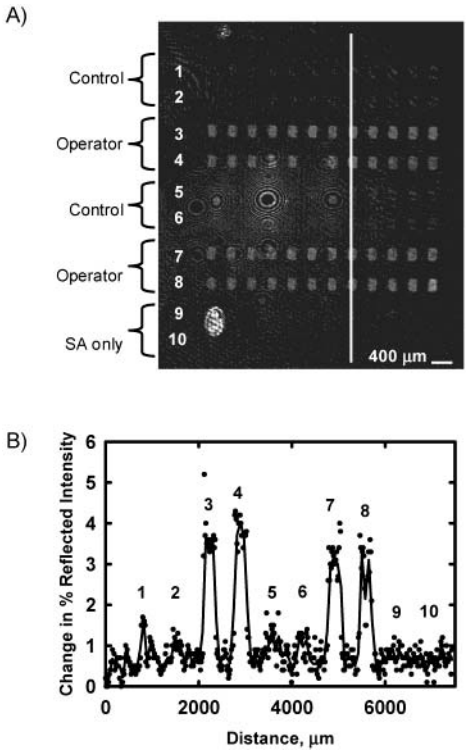

Figure 6. SPR microscope difference image and line profile showing the specific adsorption of Gal4 to the operator dsDNA array spots. (A) The difference image is the result of subtracting an image of the array prior to Gal4 adsorption from an array image after protein adsorption. All images were obtained at the same high-contrast angle. The increased intensity is due to a greater amount of Gal4 adsorption to the operator dsDNA spots compared to the SA monolayer and the control dsDNA spots. Each number identifies the location of a row that directly corresponds with the same number row in Figure 4 and Table 2. (B) The profile the line in (A) is the result of averaging the reflected intensity values for a 67-μm-wide column centered in the spots.

on the spots compared to the regions surrounding the spot (i.e., the regions without dsDNA). The differences in percent reflected intensity were averaged for each row. The average difference in percent reflected intensity for the control dsDNA spots was then used to adjust the difference in percent reflected intensity for the operator dsDNA spots to account for additional nonspecific adsorption compared to that on the surrounding region. The corrected differences in percent reflected intensity were used to calculate the Gal4 effective layer thicknesses, surface coverages, and binding ratios according to the methods outlined in ref 42. All of the values for the control dsDNA spots were calculated using the original difference in percent reflected intensity. The values are shown in Table 3. The quantitative data in Table 3 verify the qualitative observations from Figure 6. The differences in reflected intensity for the operator dsDNA spots vary from 2.6 to 2.9%, which convert to Gal4 surface densities ranging from 1.0×10^{12} to 1.2×10^{12} Gal4/cm^2, after subtraction of the amount of nonspecific binding on the control spots. The average change in reflected intensity for the control dsDNA spots was 0.4%, ~7 times less than at the operator dsDNA spots. The binding ratios were calculated using the average dsDNA packing densities for the appropriate row of operator spots from Table 2. A second binding ratio was calculated for the operator dsDNA spots using the original difference in percent reflected intensity from the image, which takes into account only the nonspecific adsorption of the surrounding regions. The binding ratios for the operator dsDNA spots were ~2.0 Gal4/dsDNA. This is in good agreement with experiments in homogeneous solution that have shown that Gal4 protein (amino acids 1−147) binds as a homodimer to its dsDNA-binding site.[61] The binding versus time curves, to be discussed further below, show a rapid initial uptake of ~15% of the saturation amount, followed by a long, relatively slow binding period at a nearly constant rate, until saturation is reached at ~500 s.

Large reflected intensity increases upon introduction of Gal4 solution and the subsequent decrease upon replacement by running buffer are observed for all surfaces in the curves in Figure 5. These changes may be due to differences in the bulk refractive index of the sample solution and the running buffer or very loosely bound Gal4 on the surface that easily rinses away. The small composition-induced difference in refractive index between the Gal4 solution and the running buffer would not have caused most of the large response observed. However, the difference in bulk refractive indexes of the two solutions due to the expected temperature difference between the Gal4 solution and the running buffer probably caused this large change in reflected intensity. It is estimated that the Gal4 solution was ~11 °C colder since the running buffer was at room temperature, but the Gal4 solution was prepared just prior to injection from a 50/50 mixture of solutions, one at room temperature and the other at 0 °C. (Direct measurement of the solution temperature inside the flow cell was not possible.) The refractive index of water is known to increase with decrease in temperature by $\sim 8 \times 10^{-5}$ RIU per degree K near room temperature.[31] Multiplying by the SPR microscope's sensitivity factor of 3900% reflected intensity/RIU, the SPR reflectivity should increase with decreasing temperature by 0.31% reflected intensity per degree K, or 3.4% for the estimated 11 °C difference. This is close to the 4% increase in reflected intensity observed between the maximum response upon Gal4 injection and after rinsing with the running buffer. Thus, it is likely that most of this increase in reflected intensity is due to this temperature difference. This highlights the importance of controlling the buffer temperature but at the same time shows the beauty of the SPR microscopy approach for effective background correction of such effects, by comparing the measured intensities with those in nearby control spots (i.e., by subtracting the intensities of these "reference spots").

Some Gal4 remains bound on the control sequence spots after buffer rinse. This indicates that there is some strong, nonspecific binding of Gal4 to the surface. Since the amount of this binding is almost exactly the same on the SA monolayer between dsDNA spots as on these control spots, this nonspecific binding is attributed to Gal4 binding to the other species present on the surface, rather than to the control dsDNA itself.

(2) Effect of High Salt Concentration on Gal4 Binding. To further investigate the binding of Gal4 protein to the operator dsDNA, we subjected the array surface with the adsorbed Gal4 to a high ionic strength solution. This high ionic strength solution should dramatically decrease the affinity of Gal4 for the dsDNA-binding site and allow the protein to be easily removed from the array spots containing the operator dsDNA. Other groups have used high ionic strength solutions to disrupt protein−dsDNA

Table 3. Gal4 Surface Coverages on the Operator and Control dsDNA Spots

spot compsn	row no.	diff in % reflected intensity[a]	SD (% reflected intensity)	corrected diff in % reflected intensity[b]	thicknes (nm)	surface density ($\times 10^{12}$ GAL4/cm^2)	binding ratio (GAL4/dsDNA)[c]	binding ratio (GAL4/dsDNA)[d]
operator dsDNA	3	2.9	0.4	2.5	0.32	1.2	1.6	1.8
	4	2.6	0.4	2.2	0.28	1.0	1.3	1.5
	7	2.7	0.3	2.3	0.30	1.1	1.3	1.6
	8	2.6	0.3	2.2	0.28	1.0	1.5	1.8
control dsDNA	1, 2, 5, 6	0.4	0.1		0.05	0.2		0.2

[a] Values found using scan mode to integrate the light intensity in a 0.04-mm^2 region in each array element and a region below the array element of the array in Figure 6 under buffer. Changes in percent reflected intensity were found by subtracting the intensity for the surrounding region from the spot intensity. The reflected intensity for each row was found by averaging the intensity values for the elements in that row. The resulting intensity values for the rows containing control dsDNA spots were averaged. Column 4 shows their spot-to-spot standard deviations (SD). [b] Calculated by adjusting the difference in percent reflected intensity using the average difference in percent reflected intensity for the Gal4 adsorption on the control dsDNA spots. [c] Calculated using the average dsDNA surface coverage for the corresponding row from Table 2. [d] Calculated using the surface density calculated from the original difference (relative to the nonspecific Gal4 adsorption on the surrounding surface) in percent reflected intensity.

interactions in order to remove the proteins from the SPR sensor surfaces to allow the surfaces to be used for additional experiments.[68] In addition, we were interested in whether we could remove the specifically bound protein upon introduction of the high ionic strength solution while leaving behind the nonspecifically bound protein.

The high ionic strength solution was prepared by diluting a 5.0 M stock solution of NaCl in Nanopure water to a concentration of 1.0 M with the running buffer. The solution was introduced to the surface at the time point indicated in Figure 5. The SPR microscope response to this solution is out of the range of the plotted reflected intensity values. After the NaCl solution was replaced with the original running buffer, the reflected intensity for all of the regions decreased to values close to the baseline values measured prior to Gal4 introduction at the beginning of the curves. This drop in the reflected intensity suggests that the high ionic strength solution removed Gal4 not only from the operator dsDNA but also from the other regions of the sensing surface. The removal of nonspecifically bound Gal4 suggests that the nonspecific interactions between the Gal4 protein and the control surfaces may be due mostly to electrostatics. This also implies that changing the ionic strength of the buffer solution possibly could decrease the amount of nonspecific binding on these surfaces. However, this is not a perfect option for studying Gal4 binding to its dsDNA-binding site because an increase in ionic strength could also change the affinity of the protein−DNA interaction.

(3) Compensation for Noise, Bulk Refractive Index Changes, and Nonspecific Binding. One advantage of using SPR microscopy for real-time, parallel analysis of protein−dsDNA interaction is the ability to simultaneously measure adsorption to binding sites and control surfaces with the same sample under the exact same experimental conditions. This allows compensation for reflected intensity changes due to certain noise sources (such as changes in intensity of the light source), bulk refractive index changes, and nonspecific adsorption that are common to the binding sites and the control sites on the sensor surface. The result of using a control surface (i.e., a "background" reference area) to compensate for these effects is shown by the difference curve in Figure 5. The adsorption curve measured for the control dsDNA area was subtracted from the curve measured for the operator dsDNA area to give the difference curve.

Background subtraction of the intensity changes for the control dsDNA removed nearly all of the intensity drop after replacement of the Gal4 solution with running buffer. The excellent compensation is shown for the reflected intensity increases due to stray light from the room reaching the CCD camera when the box containing the SPR microscope was opened in order to introduce a new sample into the flow system.

(4) Real-Time Protein−DNA Binding and Dissociation Kinetics with Background Subtraction. This subtraction method was used to obtain the Gal4 adsorption curves in Figure 7. Each curve shown was obtained by subtracting the response at a control dsDNA array spot from the response measured at a nearby operator dsDNA spot. While the microscope collected the data for all 48 operator spots simultaneously, for clarity, only six are shown here. These were selected to be characteristic of the range of responses observed. The ability to do highly sensitive, real-time adsorption measurements with fast time response in a parallel format (i.e., simultaneously in many regions of the surface) is shown clearly by these curves. The shapes of the curves are similar and verify the optimization of the fluidics system for rapid, simultaneous delivery of sample to all areas of the sensing surface. The overlap of the curves shows the ability to do accurate, real-time measurements using reference area background subtraction to remove unwanted (background) intensity changes common to both control and binding surfaces.

We can use the curves in Figure 7 to estimate the sensitivity of real-time protein adsorption measurements. Let us consider the sensitivity of these measurements. Each curve in Figure 7 corresponds to a spot of area $\sim$200 μm $\times$ 200 μm or 4×10^{-4} cm^2. With the final surface density of Gal4 from Table 3 ($\sim 1.2 \times 10^{12}$ Gal4/cm^2), this corresponds to real-time detection of $\sim 4.8 \times 10^8$ Gal4/spot at $\sim$800 s after injection in Figure 7, with a standard deviation of only $\sim$0.8% of this value and a time resolution of 1 s. Assuming a detection limit of four standard deviations,[69] we could

(68) Nagata, K.; H., H. *Real-time Analysis of Biomolecular Interactions: Applications of BIACORE*; Springer: New York, 2000.

(69) Skoog, D. A.; Leary, J. J. *Principles of Instrumental Analysis*; Saunders College Publishing: New York, 1992.

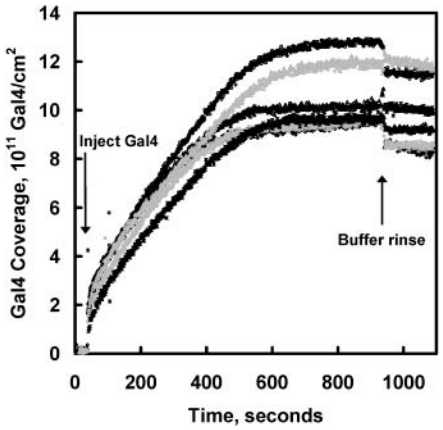

Figure 7. Simultaneous, real-time measurement of Gal4 binding to (and removal from) six representative, spatially separated areas of the dsDNA array surface, each preselected within a different spot functionalized with the Gal4 operator. Before Gal4 injection, the surface was in protein-free buffer. The adsorption/removal curves show the SPR response (reflected intensity increase/decrease) in each such array element after subtracting the response measured at a nearby control dsDNA spot, to eliminate signal contributions due to nonspecific Gal4 binding and changes in the index of refraction of the buffer solutions. The curves were obtained by integrating the reflected intensity over 200 μm $\times$ 200 μm areas within the array spots on the sensor surface for 1 s. The reflected intensity change was converted to Gal4 coverage using the methods described above for quantifying SPR microscopy data. The initial overlap of the curves shows the optimization of the fluidics to deliver sample to all areas of the surface with a fast time response.

detect $\sim 1.6 \times 10^7$ Gal4 molecules/spot ($\sim$0.5 pg of protein/spot) in this highly parallel fashion, with $\sim$100 spots/chip at a time resolution of 1 s. This corresponds to $\sim$0.5 pg of protein/spot, which is similar to the detection limits measured for adsorption of other proteins to surfaces measured with the SPR microscope.[42,55]

While the difference in reflected intensity between Gal4 binding to operator versus control sequences is small in units of absolute reflectivity ($\sim$2.7% from Table 3), this difference is large compared to the standard deviation of the measurement. Averaging over the whole chip shows that this difference is 18 times the standard deviation of intensity measurements on control DNA spots, and 7.5 times the standard deviation on operator DNA spots.

Our measured signal statistics can be used to estimate this technique's capability for spot-to-spot differentiation of small differences in protein−DNA binding stoichiometries or binding constants. The spot-to-spot relative standard deviation in Gal4 binding to operator DNA spots was 13% across the whole chip. This means that differences between two individual spots by greater than a factor of 2 in their protein−DNA binding stoichiometries or binding constants can be detected with high reliability (i.e., in >95% of the measurements). However, differences by less than a factor of 1.7 would have <95% probability of being successfully detected. Note that the above estimates are based on signals that were time-averaged for only 1 s. Better statistics could be obtained with longer signal averaging. Since the on-rate curves in Figure 7 would look exceedingly similar if they all were normalized to their maximum bound amount, it is clear too that much smaller differences in rate constants could be detected with such high reliability.

Several observations prove that most of the binding of Gal4 to the operator sequence seen in Figure 7 can be attributed to sequence-specific binding and not some nonspecific binding that is greatly different between it and the control sequence. First, the amount of Gal4 binding to the operator sequence is very close to the known stoichiometric binding ratio of 2:1 to the operator site (see above). Second, both sequences are >80 base pairs long with great variability in sequence and thus many opportunities for nonspecific binding to different sequences over the length that typically defines a protein binding site (5−20 base pairs). Finally, our earlier experiments using SPR and the same DNA immobilization chemistry but a different DNA-binding protein and different DNA sequences but of comparable length showed a similar level of nonspecific binding to a different control sequence and, again, the appropriate stoichiometry to the operator sequence.[54]

The line shapes of the Gal4 uptake curves in Figure 7 contain interesting kinetic information regarding protein−DNA binding. Since proteins of larger size adsorb at much faster rates from solutions of similar protein concentration,[60] the major portion of the uptake curves, where the binding rate (slope) is small and nearly constant and which extends from $\sim$10 to 500 s after injection, is clearly not due to diffusion limitations. The slope gives a binding rate of $\sim 3 \times 10^{-3}$ Gal4 per dsDNA per s. Dividing by the Gal4 concentration used gives a crude estimate of the on-rate constant of $\sim 3 \times 10^{-2}$ Gal4 per dsDNA per s per mg/mL Gal4 concentration, or $\sim$600 Gal4 per dsDNA per s per M Gal4 concentration. These data suggest that the selective binding of Gal4 to its immobilized operator is inherently very slow, compared, for example, to the binding of streptavidin to immobilized biotin.[60] While fitting these adsorption kinetics curves to a variety of mechanistic models would be possible, that is beyond the scope of the present paper.

The initial uptake rate of Gal4 for $\sim$15% of saturation is very rapid, with a rate comparable to that for streptavidin binding to immobilized biotin.[60] The amount of Gal 4 that rapidly rinses away upon pure buffer injection ($\sim$10% of saturation) is close to that which binds so rapidly, suggesting they have a common origin. We attribute this to weak, nonspecific binding, which may be greater in amount on the operator spots due to the greater length and difference sequence of the operator.

The average initial slope of the off-rate curves was $(1.33 \pm 0.14) \times 10^{-4}$ Gal4 per dsDNA per s, or $(6.7 \pm 0.7) \times 10^{-5}$ Gal4 homodimers per dsDNA per s, which can be considered as the effective first-order off-rate constant for Gal4 binding to its operator sequence. Dividing this by the on-rate constant of $\sim$600 Gal4 per dsDNA per s per M gives an estimate of the pseudo-first-order equilibrium dissociation for Gal4 bound to its immobilized operator sequence to be $\sim$200 nM, neglecting the dimeric character of the actual binding.

CONCLUSIONS

The kinetics of binding and dissociation of the DNA-binding protein Gal4 to an array of immobilized dsDNAs was monitored with SPR microscopy in a high-throughput, quantitative manner in real time. The binding site (operator dsDNA) for Gal4 protein was immobilized in a 10 $\times$ 12 spot array on a gold-coated glass substrate using streptavidin as a linker to tether the biotinylated dsDNA on a mixed BAT/OEG SAM. By also immobilizing spots

of a dsDNA sequence without the binding site (control dsDNA) and measuring the response *simultaneously* at all 120 array elements (operator and control), we show how a control spot can be used as a reference element to correct for changes in refractive index of the bulk solutions and nonspecific protein adsorption. We demonstrate a real-time detection limit of ~0.5 pg ($<2 \times 10^7$ molecules) of bound Gal4 protein in each 200-μm dsDNA spot on the array with 1-s time resolution. Although we used only two different dsDNA sequences for the proof of principle presented here, the results prove that these same experimental methods could be used to *simultaneously* measure protein binding to 120 different dsDNA sequences immobilized on the sensor surface, thus providing parallel, high-throughput, real-time analysis of DNA-binding proteins or the kinetics of protein−dsDNA interactions. The methods also could be extended to investigate interactions between other biomolecules.

ACKNOWLEDGMENT

This work was made possible by funding from the Institute for Systems Biology and the National Science Foundation. J.S.S-P. thanks the University of Washington Center for Nanotechnology and its NSF IGERT program for support in the form of a graduate fellowship. We thank Dr. Leroy Hood and Dr. Krassen Dimitrov for allowing us to use the robotic microspotting system in the Institute for Systems Biology Microarraying Facility and for inspiring discussions. We thank Bruz Marzolf for his assistance with the microspotting system.

Received for review October 1, 2003. Accepted January 11, 2004.

AC035159J